Biointerface Research in Applied Chemistry
Open-Access Journal (ISSN: 2069-5837)

Article
Volume 14, Issue 3, 2024, 73
https://doi.org/10.33263/BRIAC143.073

Isomer Preferences and Structural Studies on Cobaltaboranes – A Theoretical Investigation

Brindha Veerappan [1], Krishnamoorthy Bellie Sundaram [1,*]

[1] Department of Chemistry SF, PSG College of Arts and Science, Coimbatore, Tamil Nadu, India, 641014; vbrindhaveerappan@gmail.com (B.V); bskimo@yahoo.co.in (K.B.S);
* Correspondence: bskimo@yahoo.co.in (K.B.S);

Scopus Author ID 57197658621
Received: 13.05.2023; Accepted: 15.07.2023; Published: 17.02.2024

Abstract: Metallaborane is a new type of hybrid cluster with metal-boron (M-B) bonds, connecting polyhedral boranes and transition metal clusters, leading to novel structural features and diverse applications. Here we have studied the isomer preferences, electronic and geometric structural features, and spectroscopic properties of pentaborane(9) B_5H_9 (1) analogous to cobaltaboranes 1-(CpCo)B_4H_8 (2), 1-(Cp*Co)B_4H_8 (3), 2-(CpCo)B_4H_8 (4), 2-(Cp*Co)B_4H_8 (5), 1,2-(CpCo)B_3H_7 (6), 1,2-(Cp*Co)B_3H_7 (7), 2,4-(CpCo)B_3H_7 (8) and 2,4-(Cp*Co)B_3H_7 (9) where Cp=C_5H_5; Cp*=C_5Me_5, using density functional theory (DFT) methods. The computed geometries, ^{11}B, ^{1}H, and ^{13}C nuclear magnetic resonance (NMR) chemical shifts, molecular orbital (MO) analysis, and reactivity parameters are in good agreement with their stability, experimental geometry, and spectroscopic results, and, thus, highly useful in understanding the structural features of cobaltaborane clusters in a complete manner. The experimental evidence of different isomers and their stability is analyzed, and the possible structures are studied theoretically when the experimental structures are unavailable. The DFT method is once again successfully used to predict the preferred isomers and study their structural features.

Keywords: metallaborane; polyhedral borane; isomer preference; cobaltaborane; DFT; NMR.

1. Introduction

Metallaboranes are compounds that contain direct metal-boron (M-B) bonding [1]. They are true hybrid clusters that empirically join the polyhedral boranes with transition metal complexes. These metallaborane clusters are formed by obeying the cluster electron counting rules and the isolobal principle [2-5]. Boron is an important element in the periodic table and is especially well-known for its unique properties. Boron can combine with hydrogen to form boranes (B-H); when the borane molecules contain carbon atoms in their structure, they can be called carboranes (B-H, B-C) [6-9], and these carboranes are well known for their biological applications like in boron neutron capture therapy (BNCT), and drug delivery agents etc., which are proved by Prof. Hawthorns group in University of California, LA [10]. When the borane molecule combines with the metal complex, it can form metallaborane clusters. If the Metallaborane cluster (M-B) contains carbon atoms in its cluster core, then it can be called metallacarborane (M-B, B-C, M-C) [4]. These metallaboranes and metallacarboranes are also well known for their applications in material chemistry, catalysis, and biology. The metallaboranes could be *'closo'*, *'nido' 'arachno'* and *'hypo'* clusters [5] by their geometrical structures. An isolable concept in accordance with complexation theory and bonding in boranes

are used together to create new metallaborane complexes [12]. Metallaborane compounds also constitute an experimental link between transition metal clusters, borane cages, organometallic compounds, and solid-state metal boride [13].

Metallaborane chemistry is being developed as metal-ligand coordination chemistry similar to organometallic chemistry, as the metals are in low oxidation states and the 18-electron rule. However, other aspects of metallaborane chemistry more closely mimic organometallic chemistry and constitute a part of main group-transition element chemistry that gives meaning to the term "inorganometallic chemistry", i.e., metallaborane chemistry can be considered as a variation of organometallic chemistry utilizing its electron counting formalisms [1, 13, 14]. Metallaboranes arose from considering the metal atom to be an important part of the cluster skeleton. The development of Grimes's transition-metal cluster fusion reaction generated various fused boranes and carboranes. Although the principles of cluster bonding developed for main-group clusters carryover to transition-metal clusters of the group 8/9 metals with carbonyl ligands, we fully expect transition metals to exhibit variations on this cluster bonding theme as well as novel behavior not seen in main-group systems [15-19]. Several approaches to expanding cluster networks containing main groups or transition metal fragments have received considerable attention. Unfortunately, in most of the methods, the majority of metallaboranes have a low metal-to-boron ratio [20].

Cobaltaboranes were the first synthesized metallaborane sandwich-like geometry in 1973 by Russell N. Grimes and Miller. These complexes 1-[(η^5-C_5H_5)CoB_4H_8], 2-[(η^5-C_5H_5)CoB_4H_8] have been formed by the replacement of apical or basal BH vertex of pentaborane(B_5H_9) by Co(C_5H_5) unit, termed as an isolobal replacement [21- 23]. Metallaboranes are well known for group 5-9 transition metals [24-26]. Metallaboranes have important applications in many fields, including boron neutron capture therapy (BNCT), C-H activation, hydrogen storage, boron delivery agent, therapeutic agent, diagnostic agent, fogging agent, catalysis, etc. [27-39]. BNCT combines nuclear technology, chemistry, biology, and medicine to treat malignant gliomas and recurrent head and neck cancers. Practically, the lack of progress in developing more effective treatments for these tumors drives researchers to concentrate efficiently in this area of science [40, 41].

Hawthorne and his coworkers discovered that more than one BH vertices could be replaced by transition metal atoms [42, 43]. This metal-rich heterometallaborane class forms a unique path to inorgano-metallaborane chemistry [44-47]. Usually, these kinds of complexes can contribute to many applications in both industrial and biological applications. Here, we have studied the boron-rich metallaboranes, pentaborane(9) B_5H_9 (1), 1-(CpCo)B_4H_8 (2), 1-(Cp*Co)B_4H_8 (3), 2-(CpCo)B_4H_8 (4), 2-(Cp*Co)B_4H_8 (5), 1,2-(CpCo)B_3H_7 (6), 1,2-(Cp*Co)B_3H_7 (7), 2,4-(CpCo)B_3H_7 (8) and 2,4-(Cp*Co)B_3H_7 (9) using DFT (BP86/Def2-TZVP) methods, to address the isomer preferences, electronic and geometric structural features, and spectroscopic properties. Usually, the metallboranes synthesized experimentally are not completely characterized due to the problems involved, like (i) low yield of the new clusters, (ii) formation of a mixture of clusters, (iii) presence of more number of terminal and bridging hydrogens. Computational tools have proven successful in predicting the correct geometries, assigning the exact number of terminal and bridging hydrogens, and the reactivity of metallaboranes [48-50].

2. Computational Details

Computational chemistry methods are becoming important tools in assisting the complete structural characterization of compounds and also for the modeling of new compounds [51]. All the compounds in this work were studied using the following strategies: Geometry optimization, frequency calculation, NMR property calculation, molecular bonding analysis, and reactivity descriptors analysis. The academically free ORCA software developed by F. Neese and coworkers [52] has been used to perform all the density functional theory calculations in this work. Becke88 gradient correction for exchange and Perdew86 correlation within local density approximation (LDA) was used from the V-W-N parameterization [53-56]. Def2-TZVP (triple zeta valance with polarization function) basis set was used for all the molecules. In all the calculations, tight SCF convergence criteria were used [57]. Optimized geometries were checked by the following frequency calculations in order to check the obtained geometry is the minima [58, 59]. Further, the DFT-optimized geometries were used to calculate the NMR parameters like shielding constants, chemical shifts, etc., with the help of the EPRNMR module available in the ORCA software [60]. Tetramethylsilane (TMS) was used as a reference for the calculation of ^{1}H and ^{13}C NMR chemical shift values. The computed ^{11}B NMR chemical shift values were referenced to B_2H_6 as the primary reference point, and these chemical shift values (δ) were then converted to the standard $BF_3.OEt_2$ scale using the experimental value of +16.6 ppm for B_2H_6 [61, 62].

The frontier molecular orbital energies like E_{HOMO} and E_{LUMO} are used effectively to calculate the conceptual reactivity descriptors viz., The Chemical potential (μ) = $E_{LUMO + HOMO}/2$, Hardness (η) = $E_{LUMO - HOMO}/2$, Softness (S) = $1/\eta$, Electrophilicity (ω) = $\mu^2/2\Pi$. The DFT computed global reactivity descriptors have already proved to be successful in predicting the reactivities of the compounds studied and used to describe the reactive sites of these important clusters [63]. All the geometries and orbitals have been visualized using Chemcraft software [64].

3. Results and Discussion

Metallaboranes for the group 5-9 elements are well known, and the synthesis and characterization of metallaboranes, especially cobaltaboranes is an interesting field of research. Usually, these metallaboranes are synthesized by the reaction of (i) direct metal atoms and boron sources, (ii) metal complexes and boron sources like BH_3, $LiBH_4$, $NaBH_4$, etc., The characterization of these metallaboranes are always challenging. Computational tools are being practiced by chemists to address these challenges. Computational tools can aid in modeling new compounds, completing the structural characterization, studying the mechanisms involved in the reaction, analyzing the bonding, and studying the spectroscopic and thermochemical aspects. The important outcome from the density functional theory calculations on the pentaborane(9) (1), mono, and di-cobaltaboranes (2-9), studied by using the software ORCA are presented below.

3.1. Geometrical structure.

The DFT-optimized geometries at BP86/Def2-TZVP level for the clusters studied (1 - 9) are provided in Figure 1.

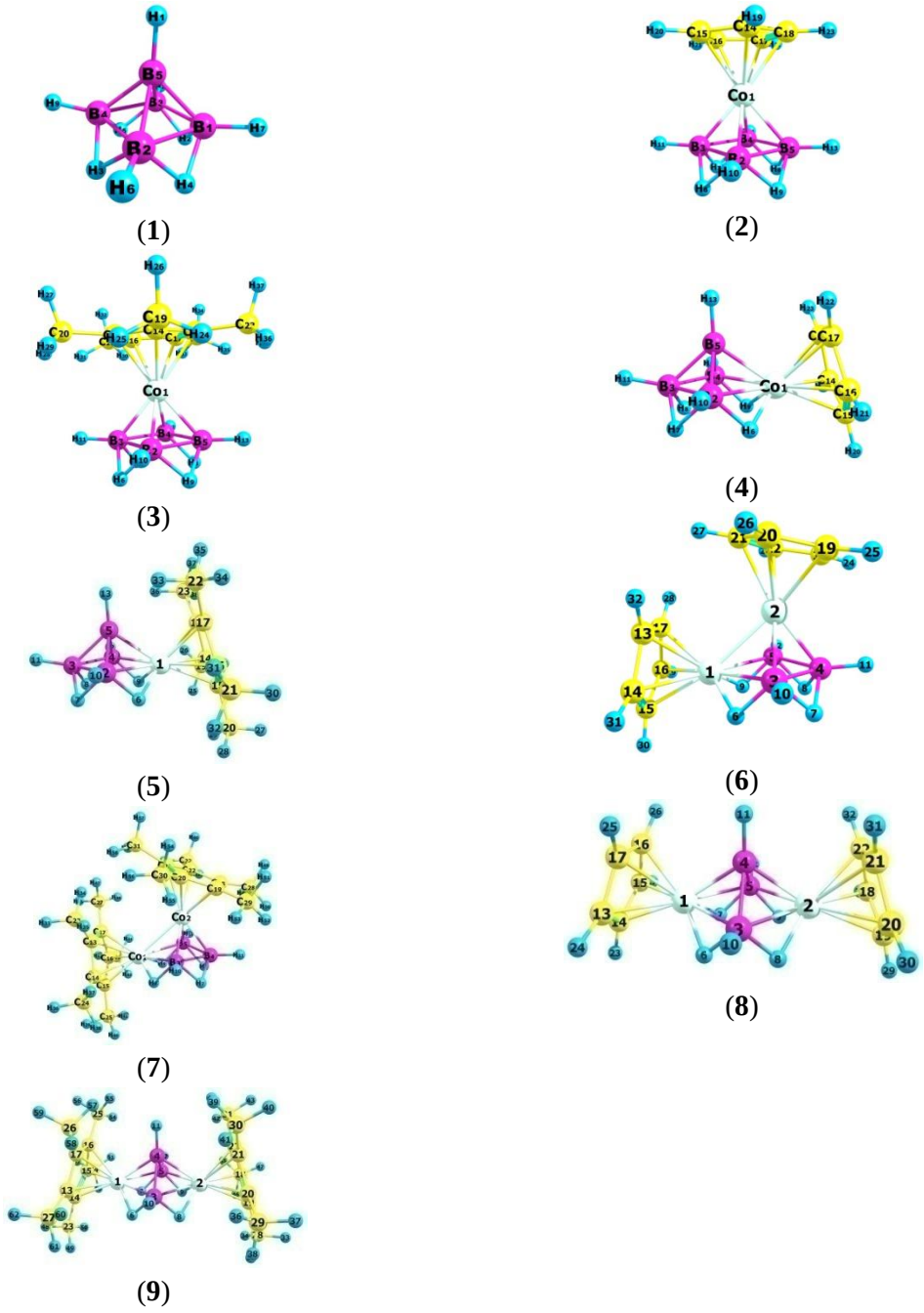

Figure 1. DFT (BP86/Def-TZVP) Optimized geometry of B_5H_9 (**1**); 1-(CpCo)B_4H_8 (**2**); 1-(Cp*Co)B_4H_8 (**3**); 2-(CpCo)B_4H_8 (**4**); 2-(Cp*Co)B_4H_8 (**5**); 1,2-(CpCo)B_3H_7 (**6**); 1,2-(Cp*Co)B_3H_7 (**7**); 2,4-(CpCo)B_3H_7 (**8**); 2,4-(Cp*Co)B_3H_7 (**9**) at (BP86/TZVP) level.

The DFT-optimized metrical parameters like bond lengths and bond angles are provided in Tables 1 to 3. The synthesis and characterization of the pentaborane(9) (1) is an important beginning of the borane cluster chemistry. The DFT computed bond parameters for the compound pentaborane(9) (1) are in good agreement with those of the experimental values obtained from X-ray crystallography. The DFT computed values are given in Table 1. The DFT computed B-B bond distance is 1.797 Å, close to the experimental value of 1.803 Å. The DFT computed B_{apical}-B_{basal} bond distance around 1.698 Å, which is close to the experimental value of 1.690 Å. As expected, the Bbasal-Bbasal-Bbasal angles are 90˚ from X-ray values, and the DFT also predicts the same.

Table 1. Metrical parameters (Å, °) obtained from DFT (BP86/Def2-TZVP) calculations for the compound Pentaborane(9) (**1**).

Atoms	Bond Length	Atoms	Bond Length & Bond Angle
B1-B2	1.796 [1.803(2)]	B1-H2	1.356 [1.352(4)]
B1-B3	1.798 [1.803(2)]	B3-H2	1.354 [1.352(4)]
B3-B4	1.797 [1.803(2)]	B3-H5	1.355 [1.352(4)]
B4-B2	1.797 [1.803(2)]	B4-H5	1.355 [1.352(4)]
B5-B1	1.698 [1.690(2)]	B4-H3	1.354 [1.352(4)]
B5-B2	1.697 [1.690(2)]	B2-H3	1.356 [1.352(4)]
B5-B3	1.698 [1.690(2)]	B2-H4	1.355 [1.352(4)]
B5-B4	1.698 [1.690(2)]	B1-H4	1.355 [1.352(4)]
B1-H7	1.191 [1.186(2)]	B2-B1-H4	83.01 [83.9]
B2-H6	1.191 [1.186(2)]	B5-B1-H7	131.90 [134.1]
B3-H8	1.191 [1.186(2)]	B1-H4-H7	107.71 [110.9]
B4-H9	1.191 [1.186(2)]	B1-B2-B3	90.01 [90.0]
B5-H1	1.191 [1.186(2)]		

The DFT computed bond parameters for the cobaltaboranes 1-(CpCo)B_4H_8 (2) and 1-(Cp*Co)B_4H_8 (3) are provided in Table 2.The DFT computed apical Co-Bbasal distances are from 1.973 – 1.975 Å. The disorder in the C_5Me_5 group in the crystal structure leads to poor refinement, which is overcome by the DFT calculations, resulting in the considerable bonding interactions between Cp* and Co groups.

Table 2. Metrical parameters (Å, °) obtained from DFT (BP86/Def2-TZVP) calculations for the compound 1-(CpCo)B_4H_8 (**2**), 1-(Cp*Co)B_4H_8 (**3**), 2-(CpCo)B_4H_8 (**4**) and 2-(Cp*Co)B_4H_8 (**5**).

Atoms	2	3	Atoms	4	5
Co1-B2	1.9744 [1.493]	1.9752	Co1-B2	2.1493	2.1493
Co1-B3	1.9728 [1.493]	1.9746	Co1-H6	1.6130	1.6130
Co1-B4	1.9730 [1.493]	1.9755	Co1-B4	2.1512	2.1512
Co1-B5	1.9753 [1.493]	1.9759	Co1-B5	2.0313	2.0313
B2-B3	1.8147 [1.834(3)]	1.8133	Co1-H9	1.6127	1.6127
B3-B4	1.8141 [1.834(3)]	1.8130	B2-B3	1.7817	1.7817
B4-B5	1.8145 [1.834(3)]	1.8138	B3-B4	1.7818	1.7818
B5-B2	1.8139 [1.834(3)]	1.8116	B2-B5	1.7209	1.7209
B2-H6	1.3534 [1.315(17)]	1.3565	B3-B5	1.7011	1.7011
B3-H6	1.3508 [1.315(17)]	1.3523	B4-B5	1.7199	1.7199
B3-H7	1.3508 [1.315(17)]	1.3523	B2-H6	1.3396	1.3396
B4-H7	1.3525 [1.315(17)]	1.3548	B2-H7	1.3486	1.3486
B4-H8	1.3512[1.315(17)]	1.3524	B3-H7	1.3546	1.3546
B5-H8	1.3534 [1.315(17)]	1.3565	B3-H8	1.3555	1.3555
B5-H9	1.3528 [1.315(17)]	1.3564	B4-H8	1.3478	1.3478
B2-H9	1.3522 [1.315(17)]	1.3537	B4-H9	1.3393	1.3393
B2-H10	1.1970 [1.121(17)]	1.1982	B2-H10	1.1988	1.1988
B3-H11	1.1970 [1.121(17)]	1.1988	B3-H11	1.1950	1.1950
B4-H12	1.1971 [1.121(17)]	1.1984	B4-H12	1.1983	1.1983
B5-H13	1.1967 [1.121(17)]	1.1978	B5-H13	1.1951	1.1951
Co1-C14	2.0891 [1.681]	2.0913	Co1-C14	2.0704	2.0704
Co1-C15	2.0747 [1.681]	2.0803	Co1-C15	2.1096	2.1096
Co1-C16	2.0708 [1.681]	2.0731	Co1-C16	2.0614	2.0614
Co1-C17	2.0807 [1.681]	2.0816	Co1-C17	2.0468	2.0468
Co1-C18	2.0922 [1.681]	2.0915	Co1-C18	2.0471	2.0471
C14-C15	1.4334 [1.401(3)]	1.4435	B2-Co1-B5	48.52	48.52
C14-H19	1.0862 [0.91(1)]	ua	B5-Co1-B4	48.46	48.46
C14-C19	ua	1.4992	B4-Co1-H9	38.44	38.44
B2-Co1-B3	54.74	54.74	B2-Co1-H6	38.44	38.49
B3-Co1-B4	54.74	54.74	H6-Co1-H9	88.06	88.06
B4-Co1-B5	54.72	54.72	Co1-B2-B3	95.90	95.90

Atoms	2	3	Atoms	4	5
B5-Co1-B2	54.68	54.68	Co1-B5-B3	103.06	103.06
B2-H6-B3	84.30 [90.6(6)]	84.04	Co1-B4-B3	95.84	95.84
B3-B2-H6	47.79	47.88	Co1-B5-H13	127.41	127.41
B3-B2-H10	134.78 [137.0(6)]	134.84	B2-B3-B5	59.17	59.17
H6-B3-H11	105.34 [108.7(6)]	105.22	B2-B5-H13	130.76	129.53
H6-B2-H9	91.47 [93.0(6)]	90.96	B3-B2-B5	58.08	62.75
Co1-B2-B3	62.58 [52.90(6)]	62.66	B2-H7-B3	82.46	82.46
B2-B3-B4	89.99 [90.0(6)]	90.0	H7-B2-B3	48.91	48.91
B2-Co1-C14	104.37	104.25	H7-B3-H8	91.75	91.76
C14-Co1-C15	40.27	40.49	C15-Co1-C16	40.16	40.16
C15-Co1-C16	40.50	40.72	Co1-C14-C15	71.52	71.52
C16-Co1-C17	40.42	40.69	H9-Co1-C14	89.98	89.98
C17-Co1-C18	40.15	40.46	B4-Co1-C18	106.81	106.81
C18-Co1-C14	40.04	40.32	B5-Co1-C17	98.44	98.44
Co1-C14-H19	124.91	Ua	H6-Co1-C16	91.02	91.02
Co1-C14-C19	ua	129.49	H9-Co1-C15	105.39	105.39

Table 3. Metrical parameters (Å, °) obtained from DFT (BP86/Def2-TZVP) calculations for the compound 1,2-$(CpCo)_2B_3H_7$ (**6**), 1,2-$(Cp^*Co)B_3H_7$ (**7**), 2,4-$(CpCo)B_3H_7$ (**8**), 2,4-$(Cp^*Co)B_3H_7$ (**9**).

Atoms	6	7	Atoms	8	9
Co1-Co2	2.4256	2.5498	Co1-B3	2.1306	2.1435 [1.986(5)]
Co1-H6	1.5827	1.5818	Co1-B4	2.0159	2.0258
Co1-B3	2.1617	2.1814	Co1-B5	2.1308	2.1434
Co1-B5	2.1702	2.1850	Co1-H6	1.6500	1.6519
Co1-H9	1.5861	1.5834	Co1-H7	1.6498	1.6511
Co2-B3	1.9890	1.9872	Co2-B3	2.1307	2.1440 [1.980(5)]
Co2-B4	1.9761	1.9766	Co2-B4	2.0155	2.0255 [1.980(5)]
Co2-B5	1.9915	1.9884	Co2-B5	2.1314	2.1442 [1.980(5)]
B3-B4	1.7997	1.8027	Co2-H8	1.6506	1.6525 [1.54(5)]
B4-B5	1.7985	1.8035	Co2-H9	1.6502	1.6511 [1.50(5)]
B3-H6	1.3391	1.3240	B3-B4	1.7708	1.7524 [1.674(9)]
B3-H7	1.3619	1.3731	B4-B5	1.7682	1.7506 [1.674(9)]
B4-H7	1.3311	1.3224	B3-H6	1.3155	1.3184 [1.29(4)]
B4-H8	1.3320	1.3224	B3-H8	1.3153	1.3182 [1.18(5)]
B5-H8	1.3605	1.3747	B5-H7	1.3157	1.3193 [1.42(5)]
B5-H9	1.3351	1.3215	B5-H9	1.3153	1.3189 [1.27(5)]
B3-H10	1.2045	1.2085	B3-H10	1.2071	1.2123 [1.19(6)]
B4-H11	1.1997	1.2011	B4-H11	1.2024	1.2086 [0.97(4)]
B5-H12	1.2046	1.2085	B5-H12	1.2062	1.2112 [1.05(7)]
Co1-C13	2.0646	2.1000	Co1-C13	2.0802	2.0760 [2.041(4)]
Co1-C14	2.0659	2.0766	Co1-C14	2.1120	2.1050 [2.059(4)]
Co1-C15	2.1025	2.0934	Co1-C15	2.0835	2.0791 [2.052(5)]
Co1-C16	2.0762	2.0795	Co1-C16	2.0518	2.0562 [2.028(4)]
Co1-C17	2.0679	2.1039	Co1-C17	2.0488	2.0580 [2.033(4)]
Co2-C18	2.0727	1.4969	Co1-H6	1.6321	1.6519 [1.67(5)]
Co2-C19	2.0727	2.0772	Co1-H7	1.6315	1.6511 [1.37(5)]
Co2-C20	2.1152	2.1379	Co2-C18	2.0845	2.0790 [2.038(4)]
Co2-C21	2.1315	2.1894	Co2-C19	2.1115	2.1048 [2.063(5)]
Co2-C22	2.1213	2.1435	Co2-C20	2.0787	2.0752 [2.033(5)]
Co1-Co2-B4	84.86	82.08	Co2-C21	2.0482	2.0582 [2.019(4)]
Co1-Co2-B3	57.63	55.83	Co2-C22	2.0519	2.0552 [2.004(5)]
Co1-Co2-B5	57.86	55.93	Co1-B4-Co2	112.075	112.84 [115.6(2)]
Co1-B5-Co2	71.15	75.15	Co1-B4-B3	68.126	68.69 [69.4(3)]
Co1-B3-Co2	71.38	75.26	Co1-H6-B3	91.143	91.68 [108(3)]
B3-Co1-H6	38.10	37.05	Co1-B4-B5	68.179	68.72 [70.7(3)]
Co1-H6-B3	95.08	96.90	Co1-H7-B5	91.157	91.68 [91(3)]
H6-Co1-H9	90.02	93.11	Co1-B5-H12	126.077	126.24
H6-B3-H7	89.70	87.88	C14-Co1-C15	39.849	40.26

Atoms	6	7	Atoms	8	9
B4-B3-H10	129.38	128.09	B5-Co1-C16	107.482	107.53
H6-B3-H10	106.23	105.54	B4-Co1-H6	87.194	86.08 [81.0]
Co2-B4-H11	122.46	121.87	B4-Co1-H7	87.112	86.12 [81.0]
C13-Co1-C14	40.69	40.51	B4-Co2-H8	87.190	86.11 [88.0(2)]
Co2-Co1-C13	98.70	110.53	B4-Co2-H9	87.086	86.04 [78.0]
H9-Co1-C15	102.29	95.33	H6-Co1-H7	84.359	84.98 [74(3)]
B5-Co2-C22	105.54	106.05	H8-Co2-H9	84.369	85.0 [78(2)]
B4-Co2-C18	101.13	95.85	B3-B4-B5	96.506	97.99 [100.6(4)]

3.2. Bonding and stability.

The DFT computed energies of the HOMO, LUMO, and the energy gap $E_{LUMO-HOMO}$ are listed in Table 4. The pictures of the frontier molecular orbitals HOMO and LUMO for the compounds 1, 2, 4, 6 & 8 are provided in Figure 2. The DFT computed energy gap $E_{LUMO-HOMO}$ value of 6.4 eV for the cluster pentaborane(9) confirms its highest stability when compared to those of clusters 2-9. From the ELUMO-HOMO values, the 1-isomers 2&3 (3 eV) is more stable than that of 2-isomers 4 & 5 (2 eV). Similarly, the 1, 2- isomers 6&7 (1.5 eV) are more stable than that of 2, 4-isomers 8 & 9 (1.0 eV) at room temperature. The DFT computed $E_{LUMO-HOMO}$ values confirm the stability of clusters 1-7 at room temperature and the formation of clusters 8, and 9 at low temperatures, suggesting their possible formation in the laboratories. From the pictures of HOMO and LUMO, the electronic cloud is delocalized throughout the molecule in the HOMO, whereas the apical B-H bond is free in the LUMO; thus, the B-H activation is facile in the apical boron. In the case of 1-(CpCo)B_4H_8(2), the LUMO is mainly contributed from the basal borons, whereas in 2-(CpCo)B_4H_8, the electrons delocalized on three borons and metal. In all cases, the stability of these molecules is revealed through electron delocalization in their frontier molecular orbitals.

Table 4. DFT computed $E_{LUMO-HOMO}$ energies, ionization potential, the heat of formation, chemical potential, hardness, softness, ionization potential, electrophilicity, and dipole moment for the compound: B_5H_9 (**1**), 1-(CpCo)B_4H_8 (**2**), 1-(Cp*Co)B_4H_8 (**3**), 2-(CpCo)B_4H_8 (**4**), 2-(Cp*Co)B_4H_8 (**5**), 1,2(CpCo)$_2B_3H_7$ (**6**), 1,2(Cp*Co)B_3H_7 (**7**), 2,4(CpCo)B_3H_7 (**8**) and 2,4(Cp*Co)B_3H_7 (**9**) at BP86/TZVP level.

Cluster	1	2	3	4	5	6	7	8	9
HOMO	-7.4770	-5.1560	-4.8328	-5.2504	-4.8539	-4.3788	-3.8574	-4.1602	--3.6738
LUMO	-1.0815	-1.8773	-1.6063	-3.1955	-2.7215	-3.0177	-2.4948	-3.1923	-2.6045
$E_{LUMO-HOMO}$	6.3955	3.2787	3.2265	2.0549	2.1324	1.3611	1.3626	0.9679	1.0693
Chemical potential(μ)	-4.2792	-3.5166	-3.2195	-4.2229	-3.7877	-3.6982	-3.1761	-3.6762	-6.2783
Hardness(η)	3.1977	1.6393	1.6132	1.0274	1.0662	0.6905	0.6813	0.4839	0.5346
Softness	0.3127	0.6100	0.6198	0.9732	0.9379	1.4695	1.4677	2.0665	1.8705
Electro-philicity(ω)	2.8632	15.0879	3.2126	8.6786	6.7279	10.0489	7.4032	13.9640	1.0694
Ionisation potential(eV)	7.4770	5.1560	4.8328	5.2504	4.8539	4.3788	3.8574	4.1602	3.6738
Electron Affinity (eV)	1.0815	1.8773	1.6063	3.1955	2.7215	3.0177	2.4948	3.1923	2.6045

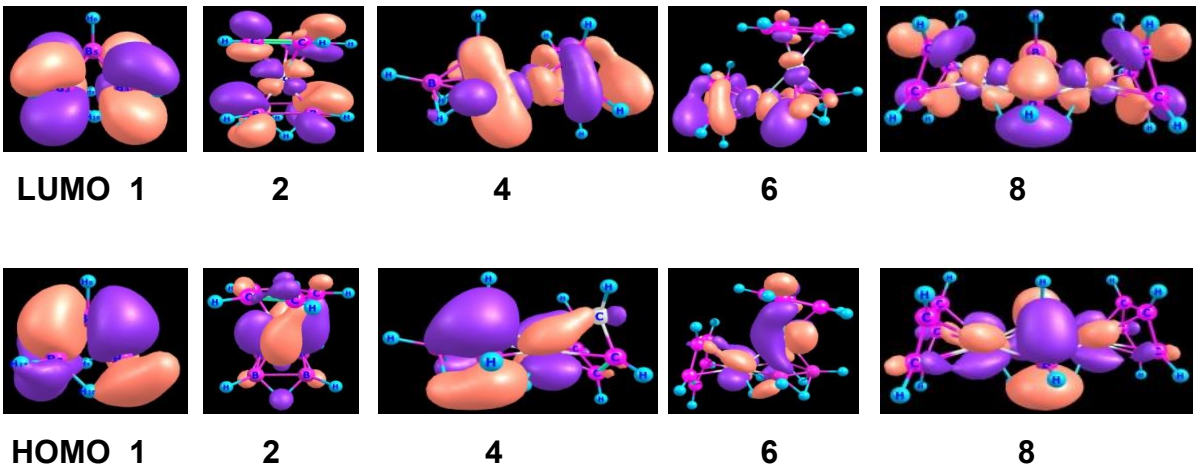

Figure 2. DFT computed pictures of HOMO and LUMO molecular orbitals of the compounds B_5H_9 (**1**), 1-(CpCo)B_4H_8 (**2**), 2-(CpCo)B_4H_8 (**4**), 1,2(CpCo)$_2B_3H_7$ (**6**) and 2,4(CpCo)B_3H_7 (**8**).

3.3. Electronic structure.

DFT calculations were made to calculate the electronic properties of the pentaborane, mono, and di-cobaltaboranes, like ionization potential, electron affinity, absolute hardness, chemical potential, and electrophilicity. All these properties are calculated from the values of HOMO and LUMO energies (Koopmann's theorem) and displayed in Table 4. Ionization potential is nothing but the energy required to remove an electron from the outermost orbital, which is equal to the energy of the HOMO. Electronic affinity can be calculated from the orbital energy of LUMO, i.e., the energy required to add an electron to the molecule. The high value of HOMO shows the electron-donating ability of an appropriate molecule of the low empty molecular orbital. From the DFT computed, E_{HOMO} values of -7.5 to -3.6 eV show the highest electron-donating ability for pentaborane(9) (1) and the least electron-donating ability for the 2,4-isomer 9.

The LUMO-HOMO energy gap is an important parameter as a function of the reactivity of the clusters. The $E_{LUMO-HOMO}$ increases, and the reactivity of the molecule decreases. The low value of $E_{LUMO-HOMO}$ suggests the reactive nature of the 2, 4-isomers 8 and 9. The hardness values are the index of stability of the molecule, and the DFT computed hardness values suggest stability decreases in the order 1 > 2, 3 > 4, 5 > 6, 7 > 8, 9 for the clusters studied. Hardness values also confirm the more stable nature of the 1-isomers 2, 3 over 2-isomers 4, 5 and 1,2-isomers 6, 7 over 2,4-isomers 8, 9 (Table 7). The electrophilicity index (ω) is a measure of the stabilization in energy after a system accepts an additional amount of electron charge from other species. The DFT computed electrophilicity values suggest the most electrophilic nature for the 1-isomer 2 (15.1eV) and the least electrophilic nature for the 2, 4-isomer 9 (1.1 eV) (Table 4). When comparing the electrophilicity of Cp Vs Cp*, as expected, the Cp analogs are more electrophilic than those of Cp* analogous.

5.4. Spectroscopic properties.

Spectroscopy is a highly efficient tool for structural characterization. Computational spectroscopic methods have played a vital role in recent years in handling the experimental discrepancies associated [48-50]. Structural characterization of metallaboranes in a complete manner has already been achieved using computational tools like DFT methods. The DFT computed ^{11}B, ^{1}H, and ^{13}C NMR chemical shift values are provided in Tables 5 to 7.

Table 5. ^{11}B, ^{1}H, and ^{13}C NMR chemical shifts obtained from DFT (BP86/Def2-TZVP) calculation for cluster B_5H_9 (**1**), 1-(CpCo)B_4H_8 (**2**).

Cluster (1)			**Cluster (2)**		
Atoms	Chemical shift		Atoms	Chemical shift	
	DFT Value	Exp. Value		DFT Value	Exp. Value
1B	-20.9	-13.4	2B	-10.3	-4.4
2B	-20.4	-13.4	3B	-10.8	-4.4
3B	-22.4	-13.4	4B	-9.7	-4.4
4B	-22.0	-13.4	5B	-12.1	-4.4
5B	-60.2	ua	$10H_{(t)}$	2.6	2.82
6H	1.3	ua	$11H_{(t)}$	2.7	2.82
7H	-2.0	-2.28	$6H_{(b)}$	-4.2	-4.30
8H	-2.0	-2.28	$7H_{(b)}$	-4.2	-4.30
9H	-2.0	-2.28	$8H_{(b)}$	-4.4	-4.30
10H	-2.1	-2.28	$9H_{(b)}$	-4.3	-4.30
11H	3.4	2.49	$12H_{(t)}$	2.6	2.82
12H	3.5	2.49	$13H_{(t)}$	2.7	2.82
13H	3.6	2.49	$19H_{Cp}$	5.6	5.01
14H	3.5	2.49	$14C_{Cp}$	86.8	83.2

In the ^{11}B NMR of the cluster pentaborane(9) 1, the four basal boron atoms resonate at -13.4 ppm experimentally, and the DFT predicts that these borons resonate at -20.4, -20.9, -22.4, and -22.0 ppm. Interestingly, the peak for the apical boron atom was not observed experimentally, and DFT predicts that the signal at -60.4 ppm corresponds to the apical boron, which is highly shielded when compared to that of basal borons. In the ^{1}H NMR of the pentaborane, all the bridging hydrogen atoms resonate around -2.0 ppm from the DFT computations, and the corresponding experimentally observed values are around -2.28 ppm. Interestingly, four terminal hydrogen atoms resonate around 3.4 ppm and only one at 1.3 ppm, from the DFT computations, whereas the experimentally observed value for the terminal hydrogens is 2.49 ppm. Thus DFT is clearly helping to observe the terminal hydrogen of the apical boron at a higher field when compared to that of the terminal hydrogens of the basal boron atoms.

Table 6. ^{11}B, ^{1}H, and ^{13}C NMR chemical shifts obtained from DFT (BP86/TZVP) calculation for cluster 1-(Cp*Co)B_4H_8 (**3**), 2-(CpCo)B_4H_8 (**4**), 2-(Cp*Co) B_4H_8 (**5**) and 1,2-$(CpCo)_2B_3H_7$ (**6**).

Cluster (3)		**Cluster (4)**		**Cluster (5)**		**Cluster (6)**	
Atoms	**Chemical shift**	**Atoms**	**Chemical shift**	**Atoms**	**Chemical shift**	**Atoms**	**Chemical shift**
2B	-11.4	2B	-21.0	2B	-19.8	3B	1.5
3B	-9.2	4B	-8.3	5B	-8.3	5B	1.6
4B	-10.1	5B	-20.9	4B	-19.9	4B	0.8
5B	-9.7	3B	1.2	3B	-3.4	$10H_t$	3.6
$10H_t$	2.3	$10H_t$	2.2	$9H_t$	2.2	$11H_t$	3.2
$11H_t$	2.4	$11H_t$	2.8	$11H_t$	2.2	$12H_t$	3.6
$6H_b$	-4.2	$12H_t$	2.2	$10H_t$	3.2	$6H_b$	-14.1
$7H_b$	-4.0	$7H_b$	-2.9	$7H_b$	-2.9	$7H_b$	-3.5
$8H_b$	-3.9	$8H_b$	-2.9	$8H_b$	-2.8	$8H_b$	-3.7
$9H_b$	-3.9	$9H_b$	-10.1	$6H_b$	-9.1	$9H_b$	-13.7
$12H_t$	2.3	$6H_b$	-9.7	$9H_b$	-8.7	23H	6.4
$13H_t$	2.3	$13H_t$	3.4	$13H_t$	2.1	24H	5
24H	2.3	19H	2.9	24H	1.39	27H	6.6
25H	1.9	20H	5.8	27H	3.35	28H	4.5
35H	2.0	21H	4.9	30H	1.37	31H	5
36H	1.8	22H	4.2	33H	1.89	13C	79.8
14C	103.4	23H	4.55	36H	1.521	14C	86.3
15C	102.7	14C	89.2	14C	102.4	15C	92.2

Cluster (3)		Cluster (4)		Cluster (5)		Cluster (6)	
Atoms	**Chemical shift**	**Atoms**	**Chemical shift**	**Atoms**	**Chemical shift**	**Atoms**	**Chemical shift**
19C	13.8	15C	90.8	15C	103.09	18C	83.8
20C	13.1	16C	89.7	17C	97.2	20C	90.8
21C	14.0	17C	83.5	19C	14.0	21C	96.9
22C	13.7	18C	81.7	21C	13.2	22C	91.7

The four basal boron atoms of cluster 1-(CpCo)B_4H_8 (2) resonate around -9.7 ppm to -12.1 ppm from the DFT calculations, and the corresponding experimentally observed value is -4.4 ppm. The terminal hydrogens resonate around 2.6 ppm and 2.7 ppm from the DFT calculations, and the corresponding experimentally observed values are 2.82 ppm. In the ^{13}C NMR, experimentally, the hydrogens of the cyclopentadienyl group resonate around 83.2 ppm, which is close to the values around 86.4 ppm calculated from the DFT method. In the Cp* analog, 1-(Cp*Co)B_4H_8 (3), the four basal borons resonate around -9.2 ppm To -11.4 ppm (DFT).

Table 7. ^{11}B, ^{1}H, and ^{13}C NMR chemical shifts obtained from DFT (BP86/Def2-TZVP) calculation for cluster 1,2-(Cp*Co) B_3H_7 (**7**), 2,4-(CpCo) B_3H_7 (**8**) and 2,4-(Cp*Co) B_3H_7 (**9**).

Cluster (7)		Cluster (8)		Cluster (9)	
Atoms	**Chemical shift**	**Atoms**	**Chemical shift**	**Atoms**	**Chemical shift**
3B	11.54	3B	-19.8	1B	-19.2 [-18.1]
4B	11.63	4B	81.1	2B	77.3 [65.8]
5B	11.60	5B	-4.3	3B	-19.1 [-18.1]
$6H_b$	-12.59	$6H_b$	-8	$3H_t$	4.7 [6.28]
$7H_b$	-2.96	$7H_b$	-8	$4H_b$	0.7 [-12.7]
$8H_b$	-2.97	$8H_b$	-8.1	$5H_b$	0.7 [-12.7]
$9H_b$	-13.72	$9H_b$	-6.9	$6H_b$	-8.2 [-12.7]
$10H_t$	3.38	$10H_t$	1.3	$7H_b$	-7.1 [-12.7]
$11H_t$	2.64	$11H_t$	6.2	$8H_t$	1.7 [6.28]
$12H_t$	1.35	$12H_t$	1.2	$9H_t$	8.2 [6.28]
13C	112.39	23H	5.9	32H	2.1 [1.7]
18C	117.2	29H	5.8	12C	95.1 [89.6]
23C	11.39	13C	91.3	22C	11.8 [10.3]
28C	11.97	18C	96.7		
33H	1.38				
48H	1.31				

In the dicobaltaborane cluster 2,4-(Cp*Co) B_3H_7 (9), two boron signals with a 2:1 ratio are expected. The two basal boron atoms connected to the two cobalt atoms resonate at -19.1, and -19.2 ppm apical boron atom resonates at 77.3 ppm from the DFT calculations at BP86/Def2-TZVP level of theory. The corresponding experimentally observed values are -18.1 ppm for the basal borons and 65.8 ppm for the apical boron. As expected, the apical boron is less shielded and resonates at a lower field, whereas the basal borons are highly shielded and resonate at a higher field when compared to that of the apical boron atom. In the ^{1}H NMR spectrum, the four bridging hydrogen atoms resonate at 0.7 ppm, 0.7 ppm, -7.1 ppm, and –8.2 ppm, whereas experimentally, a broad peak was observed at -12.7 ppm. The three hydrogens resonate at 1.7 ppm, 4.7 ppm, and 8.2 ppm from the DFT calculations, and the corresponding experimental value is 6.28 ppm. In the 13C NMR spectrum, two signals were observed at 89.6 ppm and 10.3 ppm experimentally, and the corresponding DFT computed values are 95.1 ppm and 11.8 ppm. Thus, the DFT computed chemical shift values are close to those of the experimentally observed values.

4. Conclusions

DFT calculations were carried out on the pentaborane(9) (1) and its analogs of mono- and di-cobaltaboranes 1-(CpCo)B_4H_8 (2), 1-(Cp*Co)B_4H_8 (3), 2-(CpCo)B_4H_8 (4), 2-(Cp*Co)B_4H_8 (5), 1,2-(CpCo)B_3H_7 (6), 1,2-(Cp*Co)B_3H_7 (7), 2,4-(CpCo)B_3H_7 (8) and 2,4-(Cp*Co)B_3H_7 (9) to study their geometrical and electronic structural features, stability, isomer preferences, and spectroscopic properties.

The following conclusions were drawn from the present study: DFT calculations using ORCA at BP86/def2-TZVP level predict the structural parameters for the compoundpentaborane(9) 1, which are in good agreement with the experimental values. DFT-optimized geometries for the pentaborane(9) (1) analogs of mono-cobaltaboranes 2-5 resulted in minima, and the bond parameters are in good agreement with the experimental values. The DFT computed geometries support the geometries proposed in the solution and are comparable to similar compounds, suggesting the possible synthesis of compounds 2-5. DFT-optimized geometries for the pentaborane(9) (1) analogs of di-cobaltaboranes 6-9 also resulted in minima, and the bond parameters are in good agreement with the experimental values. The DFT computed geometries support the geometries proposed in the solution and are comparable to similar compounds, suggesting the possible synthesis of compounds 6-9.

DFT computed energetics is useful in ascertaining the stability of the isomers studied. The DFT computed $E_{LUMO-HOMO}$ of the monocobaltaboranes suggests the more stable nature of the 1-isomers 2, 3 than those of 2-isomers 4, 5. Similarly, DFT predicts that the 1, 2-isomers of the dicobaltaboranes 6, 7 are more stable than 2, 4-isomers 8, 9 at room temperature.

The ^{1}H, ^{13}C, and ^{11}B NMR chemical shifts computed at DFT (BP86/TZVP) level are in close agreement with the experimentally observed values for clusters 1, 2, and 9. The DFT computed ^{1}H, ^{13}C, and ^{11}B NMR chemical shift values also supporting the geometries proposed in the solution and comparable to the similar compounds 3-7. DFT also computes the ^{11}B NMR chemical shifts which are not observed experimentally; for example, the apical boron of cluster 1 resonates at -60.2 ppm, a higher field that is not observed experimentally. DFT-optimized geometries and the computed ^{1}H, ^{13}C, and ^{11}B NMR chemical shift values are very useful in successfully assigning the number and position of the bridging and terminal hydrogens of clusters 1-9.

Funding

This research was funded by PSG Management Trust, Coimbatore, Seed Grant No: PSGCAS/IRSG/2021-2022/Chemistry/028.

Acknowledgments

Declared none.

Conflicts of Interest

The authors declare no conflict of interest.

References

1. Fehlner, T. P.; Halet, J-F.; Saillard, J-Y. Molecular Clusters. A Bridge to Solid State Chemistry, Cambridge University Press, New York, **2007,** https://doi.org/10.1017/CBO9780511628887.

2. Housecroft, C. E. *Inorganometallic Chemistry* (Ed.: T. P. Fehlner), Plenum, New York, **1992**, https://doi.org/10.1007/978-1-4899-2459-9_3.
3. Grimes, R. N. Metallacarboranes and metal-boron clusters in organometallic synthesis, *Pure Appl. Chem*, **1982**, *54*, 43 – 58, http://dx.doi.org/10.1351/pac198254010043.
4. Rudolph, R. W. Boranes and heteroboranes: a paradigm for the electron requirements of clusters? *Acc. Chem. Res*, **1976**, *9*, 446-452, https://doi.org/10.1021/ar50108a004.
5. Wade, K. Structural and Bonding Patterns in Cluster Chemistry, *Adv. Inorg. Chem. Radiochem*, **1976**, *18*, 1, https://doi.org/10.1016/S0065-2792(08)60027-8.
6. Bauer, S. H. The Structure of Diborane, *J. Am. Chem. Soc*. **1937**, *59*, 1096, https://doi.org/10.1021/ja01285a041.
7. Goszczynski, M.; Fink, K.; Boratynski, J. Icosahedral boron clusters as modifying entities for biomolecules, *Expert Opinion On Biological Therapy* **2018**, *18*, 205–213, https://doi.org/10.1080/14712598.2018.1473369.
8. Farras, P.; Juarez Perez, E. J.; Lepsik, M. Metallacarboranes and their interactions: theoretical insights and their applicability. *Chem. Soc. Rev*, **2012**, *41*, 3445–3463, https://doi.org/10.1039/c2cs15338f.
9. Borthakur, R.; Kar, S.; Barik, S. K. ; Bhattacharya, S.; Kundu, G.; Varghese, B.; Ghosh, S. Synthesis, Chemistry, and electronic structures of group 9 metallaboranes. *Inorg. Chem*, **2017**, *56*, 1524-1533, https://doi.org/10.1021/acs.inorgchem.6b02626.
10. Hawthorne, M. F.; Maderna, A. Applications of radiolabeled boron clusters to the diagnosis and treatment of cancer. *Chem. Rev*, **1999**, *99*, 3421−3434, https://doi.org/10.1021/cr980442h.
11. K. Pathak, C. Nandi, J. F. Halet, S. Ghosh, Metal-rich metallaboranes: synthesis, structures and bonding of bi- and trimetallic open-faced cobaltaboranes, *Inorganics* **2021**, *9*, 28, https://doi.org/10.3390/inorganics9040028.
12. Kar, S.; Pradhan, A. N.; Ghosh, S. Metal-rich metallaboranes: Clusters containing triply and tetra bridging borylene and boride units. *Coordination Chemistry Rev* **2021**, *436*, 213796, https://doi.org/10.1016/j.ccr.2021.213796.
13. Fehlner, T. P. Metallaboranes, Structural and Electronic Paradigms in Cluster Chemistry **2006**, https://doi.org/10.1007/BFb0018028.
14. Chakrahari, K. K.V.; Sharmila, D.; Barik, S. K.; Mondal, B.; Varghese, B.; Ghosh, S. Hypoelectronic metallaboranes: Synthesis, structural characterization and electronic structures of metal-rich cobaltaboranes. *J. Organometallic Chem*. **2014**, *749*, 188-196, https://doi.org/10.1016/j.jorganchem.2013.09.032.
15. Zafar, M.; Ramalakshmi, R.; Ahmad, A.; Sudhadevi Antharjanam, P. K.; Bontemps, S.; Sabo-Etienne, S.; Ghosh, S. Cooperative b–h and si–h bond activations by κ^2-*n*,*s*-chelated ruthenium borate complexes. *Inorganic Chemistry*. **2021**, *60*, 1183-1194, https://doi.org/10.1021/acs.inorgchem.0c03306.
16. Grimes, R. N. Role of metals in borane clusters *Accounts of Chemical Research* **1983,** *16*, 22-26, https://doi.org/10.1021/ar00085a004.
17. Roy, D. K.; Jagan, R.; Ghosh, S. Fused metallaborane clusters of group 9 and 8 transition metals. *J. Organometallic Chem*, **2014**, *772-773*, 242-247, https://doi.org/10.1016/j.jorganchem.2014.09.023.
18. Borthakur, R.; Prakash, R.; Nandi, P.; Ghosh, S. Metal rich metallaboranes of group 9 transition metals. *J. Organometallic Chem*, **2016,** *825-826*, 1-7, https://doi.org/10.1016/j.jorganchem.2016.10.008.
19. Kar, S.; Pradhan, A. N.; Ghosh, S. Comprehensive Organometallic Chemistry IV (Fourth Edition), **2022**, *9*, 263-369, https://doi.org/10.1016/B978-0-12-820206-7.00169-4.
20. Lei, X.; Shang, M.; Fehlner, T. P. Chemistry of dimetallaboranes derived from the reaction of $[Cp^*MCl_2]_2$ with monoboranes (M = Ru, Rh; Cp* = η^5-C_5Me_5). *J. Am. Chem. Soc* **1999**, *121*, 1275, https://doi.org/10.1021/ja982954j.
21. Bose, S. K.; Ghosh, S. Novel 11-vertex, 11-skeletal electron pair tantalaborane of unusual shape. *Organometallics* **2011**, *30*, 4788, https://doi.org/10.1021/om200514t.
22. Miller, V. R.; Grimes, R. N. Synthesis of four-, five-, and six-boron metallocarboranes from polyhedral dicarbaheptaborane ($C_2B_5H_7$). *J. Am. Chem. Soc* **1973**, *95*, 5078, https://doi.org/10.1021/JA00790A014.
23. Venable, T. L.; Sinn, E.; Grimes, R. N. 1-[(η^5-C_5R_5)Co]B_4H_8(R = H or Me) sandwich complexes containing a square cyclic $B_4H_8^{2-}$ ligand analogous to $C_4H_4^{2-}$: structural and spectroscopic studies. *J. Chem. Soc. Dalton Transactions* **1984**, 2275-2279, https://doi.org/10.1039/DT9840002275.
24. Fehlner, T. P. Exploring the interactions of d-block elements with boron. A case for electronically unsaturated metallaborane clusters. *J. Chem. Soc. Dalton Trans*. **1998**, *1525*, https://doi.org/10.1039/A800924D.
25. Ghosh, S.; Rheingold, A. L.; Fehlner, T. P. Metallaboranes of the earlier transition metals. An arachno nine-vertex, nine-skeletal electron pair rhenaborane of novel shape: importance of total vertex connectivities in such systems. *Chem. Commun* **2001**, *895*, https://doi.org/10.1039/B101918J.
26. Ghosh, S.; Noll, B. C.; Fehlner, T. P. Synthesis and Characterization of [*exo*-$BH_2(Cp^*M)_2B_9H_{14}$] (M=Ru, Re), and the Conversion of the Ruthenaborane into $[(Cp^*Ru)_2B_{10}H_{16}]$ with an Open Cluster Framework Based on a Capped Truncated Tetrahedron. *Angew. Chem. Int. Ed* **2005**, *44*, 2916, https://doi.org/10.1002/anie.200500343.
27. Issa, F.; Kassiou, M.; Rendina, L. M. Boron in Drug Discovery: Carboranes as Unique Pharmacophores in Biologically Active Compounds. *Chem. Rev* **2011**, *111*, 5701. https://doi.org/10.1021/cr2000866.
28. Barth, R. F.; Mi, P.; Yang, W.; Barth, Boron delivery agents for neutron capture therapy of cancer. *Cancer.*

Commun. **2018,** *38*, 35, https://doi.org/10.1186/s40880-018-0299-7.
29. Kirkina, V. A.; Kissel, A. A.; Selikhov, A. N.; Nelyubina, Y. V.; Filippov, O. A.; Belkova, N. V.; Trifonov, A. A.; Shubina, E. S. Amine-boranes reactions promoted by lanthanide(II) ions, *Chem. Commun***,** **2022**, *58***,** 859-862, https://doi.org/10.1039/D1CC06401K.
30. Banjade, H.; Fang, H.; Jena, P. Metallo-boranes: a class of unconventional superhalogens defying electron counting rules, *Nanoscale*, **2022**, *14***,** 1767-1778, https://doi.org/10.1039/D1NR06929B.
31. Bose, S. K.; Geetharani, K.; Ghosh, S. C–H activation of arenes and heteroarenes by early transition metallaborane, $[(Cp^*Ta)_2B_5H_{11}]$ (Cp^* = η^5-C_5Me_5). *Chem. Comm*, **2011**, *47*, 11996–11998, https://doi.org/10.1039/C1CC15394C.
32. Mboyi, C. D.; Poinsot, D.; Roger, J.; Fajerwerg, K.; Kahn, M. L.; Hierso, J. C. The hydrogen-storage challenge: nanoparticles for metal-catalyzed ammonia borane dehydrogenation. *Small, Wiley-VCH Verlag* **2021**, 2102759, https://doi.org/10.1002/smll.202102759.
33. Gama, M.; Silva, X. A.; Doan, T. H.; Osi, A.; Chardon, A.; Tumanov, N.; Wouters, J.; Berionni, G. Triptycene boronates, boranes, and boron ate-complexes: toward sterically hindered triarylboranes and trifluoroborates. *Eur. J. Org. Chem* **2021**, 1440–1445, https://doi.org/10.1002/ejoc.202001672.
34. Akbarzadeh, A. R.; Vrinceanu, D.; Tymczak, C. J. Department of Physics, Texas Southern University, Houston, Texas 77004, USA. Metalloboranes for high density hydrogen storage, Patent Application Publication May 25, **2017**. Sheet 1 of 6 US 2017/O145036A1, https://patents.google.com/patent/US20170145036A1/en.
35. Aubry, B.; Canterel, R.; Lansalot, M.; Bourgeat-Lami, E.; Airoudj, A.; Graff, B.; Dietlin, C.; Morlet-Savary, F.; Blahut, J.; Benda, L.; Pintacuda, G.; Lacote, E.; Lalevee, J. Development of a borane–(meth)acrylate photo-click reaction. *Angewandte Chemie International Edition* **2021**, *60*, 17037-17044, https://doi.org/10.1002/anie.202103008.
36. Kirschner, S.; Peters, M.; Yuan, K.; Uzelac, M.; Ingleson, M. Developing organoboranes as phase transfer catalysts for nucleophilic fluorination using CsF. *Chem. Sci* **2022**, *13*, 2661-2668, http://xlink.rsc.org/?DOI=d2sc00303a.
37. Wang, H.; Xie, Z. Synthesis and reactivity of carboranylsilylene stabilized boranes: construction of carborane-fused silaboracycles. *Organometallics* **2021**, *40*, 3819–3824, https://doi.org/10.1021/acs.organomet.1c00526. .
38. Guennic, B. L.; Jiao, H.; Kahlal, S.; Saillard, J.-Y.; Halet, J.-F.; Ghosh, S.; Shang, M.; Beatty, A. M.; Rheingold, A. L.; Fehlner, T. P. Synthesis and characterization of hypoelectronic rhenaboranes. analysis of the geometric and electronic structures of species following neither borane nor metal cluster electron-counting paradigms. *J. Am. Chem. Soc* **2004**, *126*, 3203-3217, https://doi.org/10.1021/ja039770b.
39. Dai, Y. Huang, J. Zhu. Predicting dinitrogen activation by carborane-based frustrated lewis pairs. *Organometallics* **2022,** *41*, 1480-1487, https://doi.org/10.1021/acs.organomet.2c00069.
40. Fan, C. H.; Wang, T. W.; Hsieh, Y. K.; Wang, C. F.; Gao, Z.; Kim, A.; Nagasaki, Y.; Yeh, C. K. Enhancing boron uptake in brain glioma by a boron-polymer/microbubble complex with focused ultrasound. *ACS Appl. Mater. Interfaces* **2019**, *1112*, 11144-11156, https://doi.org/10.1021/acsami.8b22468.
41. Lesnikowski, Z. J.; Paradowska, E.; Olejniczak, A. B.; Studzinska, M.; Seekamp, P.; Schubler, U.; Gabel, D.; Schinazic, R. F.; Pleseke, J. Towards new boron carriers for boron neutron capture therapy: metallacarboranes and their nucleoside conjugates. *Bioorganic & Medicinal Chemistry*, **2005**, *13*, 4168–4175, https://doi.org/10.1016/j.bmc.2005.04.042.
42. Hawthorne, M. F. Chemistry of the polyhedral species derived from transition metals and carboranes. *Acc. Chem. Res* **1968**, *1*, 281− 288, https://doi.org/10.1021/ar50009a004.
43. Callahan, K. P.; Hawthorne, M. F. Ten years of metallocarboranes. *Adv. Organomet. Chem*, **1976**, *14*, 145−186, https://doi.org/10.1016/S0065-3055(08)60651-6.
44. Pradhan, A. N.; Rout, B. K.; Halet, J.-F.; Ghosh, S. Metal-rich clusters: synthesis, structure and bonding of metallaboranes featuring μ_5-boride and triply bridging borylene units. *Inorganica Chimica Acta* **2022,** *540*, 121045, https://doi.org/10.1016/j.ica.2022.121045.
45. Bag, R.; Gomosta, S.; Pradhan, A. N.; Roisnel, T.; Ghosh, S. Synthesis and characterization of group 6-9 metal-rich homo- and hetero-metallaboranes. *J. Indian Chemical Soc* **2021**, *98*, 100040, https://doi.org/10.1016/j.jics.2021.100040.
46. Gomosta, S.; Kar, S.; Pradhan, A. N.; Bairagi, S.; Ramkumar, V.; Ghosh, S. Synthesis, structures, and bonding of metal-rich metallaboranes comprising triply bridging borylene and boride moieties. *Organometallics* **2021**, *40*, 529−538, https://dx.doi.org/10.1021/acs.organomet.0c00780.
47. Prakash, R.; Pradhan, A. N.; Jash, M.; Kahlal, S. ; Cordier, M.; Roisnel, T.; Halet, J-F.; Ghosh, S. Diborane(6) and its analogues stabilized by mono-, bi-, and trinuclear group 7 templates: combined experimental and theoretical studies. *Inorganic Chem* **2020**, *59*, 1917-1927, https://doi.org/10.1021/acs.inorgchem.9b03217.
48. Nagalakshmi, V.; Nandhini, R.; Brindha, V.; Krishnamoorthy, B. S.; Balasubramani, K. Half-sandwich ruthenium(II) complexes containing biphenylamine based Schiff base ligands: Synthesis, structure and catalytic activity in amidation of various aldehydes. *J. Organometallic Chem*, **2020**, *912*, 121175, https://doi.org/10.1016/j.jorganchem.2020.121175.

49. Almansour, A. I.; Arumugam, N.; Soliman, S. M.; Krishnamoorthy, B. S.; Halet, J-F. Vishnu Priya, R.; Suresh, J.; Al-thamili, D. M.; Al-aizari, F. A.; Suresh Kumar, R. Stereoselective synthesis, structure and DFT studies on fluoro- and nitro- substituted spirooxindole-pyrrolidine heterocyclic hybrids. *J. Molecular Struc* **2021**, *1237*, 130396, https://doi.org/10.1016/j.molstruc.2021.130396.
50. Krishnamoorthy, B. S.; Thakur, A.; Chakrahari, K. K. V.; Bose, S. K.; Hamon, P. ; Roisnel, T.; Kahlal, S.; Ghosh, S.; Halet, J-F. Theoretical and experimental investigations on hypoelectronic heterodimetallaboranes of group 6 transition metals. *Inorg. Chem* **2013**, *51*, 10375-10383, https://doi.org/10.1021/ic301571e.
51. Patel, T. R.; Ganguly, B. Exploring the metal-free catalytic reduction of CO_2 to methanol with saturated adamantane scaffolds of phosphine-borane frustrated Lewis pair: A DFT study. *J. Molec. Graphic. Model* **2022**, *113*, 108150, https://doi.org/10.1016/j.jmgm.2022.108150**. .**
52. Neese, F. The ORCA program system. *WIREs Wiley Interdiscip. Rev. Comput. Mol. Sci*. **2022**, https://doi.org/10.1002/wcms.1606.
53. Vosko, S. H.; Wilk, L.; Nusair, M. Accurate spin-dependent electron liquid correlation energies for local spin density calculations: a critical analysis. *Can. J. Phys*. **1980**, *58*, 1200-1211, http://dx.doi.org/10.1139/p80-159.
54. Becke, A. D. Density functional calculations of molecular bond energies. *J. Chem. Phys*. **1986**, *84*, 4524-4529, https://doi.org/10.1063/1.450025.
55. Becke, A. D. Density-functional exchange-energy approximation with correct asymptotic behavior. *Phys. Rev. A* **1986**, *38*, 3098-3100, https://doi.org/10.1103/PhysRevA.38.3098.
56. Perdew, J. P. Density-functional approximation for the correlation energy of the inhomogeneous electron gas. *Phys. Rev. B*, **1986**, *33*, 8822-8824. https://doi.org/10.1103/PhysRevB.33.8822.
57. Weigend, F.; Ahlrichs, R. Balanced basis sets of split valence, triple zeta valence and quadruple zeta valence quality for H to Rn: Design and assessment of accuracy. *Phys. Chem. Chem. Phys*, **2005**, *7*, 3297-3305, https://doi.org/10.1039/b508541a.
58. Reveles, J. U.; Koster, A. M. Geometry optimization in density functional methods. *J. Comput. Chem*, **2004**, *25*, 1109 –1116, https://doi.org/10.1002/jcc.20034.
59. Schlegel, H. B. Geometry optimization. *WIREs Comput. Mol. Sci* **2011**, *1*, 790–809, https://doi.org/10.1002/wcms.34.
60. Mares, J.; Vaara, J. *Ab initio* paramagnetic NMR shifts *via* point-dipole approximation in a large magnetic-anisotropy Co(II) complex. *Phys. Chem. Chem. Phys* **2018**, *20*, 22547, https://doi.org/10.1039/C8CP04123G.
61. E. D. Becker. High Resolution NMR (Third Edition). *Theo. Chem. App* **2000**, 83-117, https://toukach.ru/files/nmr_becker.pdf.
62. Guzman, A. L.; Hoye, T. R. TMS is superior to residual C*H*Cl_3 for use as the internal reference for routine ^{1}H NMR spectra recorded in $CDCl_3$. *J. Org. Chem*, **2022**, *87*, 905–909, https://doi.org/10.1021/acs.joc.1c02590.
63. Oller, J.; Perez, P.; Ayers, P. W.; Vohringer-Martinez, E. Global and local reactivity descriptors based on quadratic and linear energy models for *α,β*-unsaturated organic compounds. *Int. J. Quantum. Chem* **2018**, *118*, 25706, https://doi.org/10.1002/qua.25706.
64. Chemcraft - Graphical program for visualization of quantum chemistry computations (chemcraftprog.com). https://www.chemcraftprog.com/.